Fraunhofer-like diffracted lateral photoelectron momentum distributions of H_{2}^{+} in charge-resonance-enhanced ionization in strong laser fields

Lin Xin, Han-Cheng Qin, Wan-Yang Wu, and Feng He

Phys. Rev. A **92**, 063803 — Published 3 December 2015

DOI: 10.1103/PhysRevA.92.063803

Fraunhofer-like diffracted lateral photoelectron momentum distributions of H_2^+ in charge-resonance enhanced ionization in strong laser fields

Lin Xin[1,2], Han-Cheng Qin[1], Wan-Yang Wu[1], and Feng He[1*]
[1] *Key Laboratory for Laser Plasmas (Ministry of Education) and Department of Physics and Astronomy, Collaborative innovation center of IFSA (CICIFSA), Shanghai Jiao Tong University, Shanghai 200240, China*
[2] *Zhiyuan colledge, Shanghai Jiao Tong University, Shanghai 200240, China*
(Dated: November 9, 2015)

For H_2^+ at the critical internuclear distance where the charge-resonance enhanced ionization is most prominent, the lateral photoelectron momentum distribution presents the Fraunhofer-like diffraction pattern: a central disk surrounded by one or more rings. We study this phenomenon by simulating the time-dependent Schrödinger equation and unveil the mechanism: the stretched molecule constructs an interatomic Coulomb potential, which works as a circular aperture and diffracts the electron when it travels between two nuclei. This distinct lateral photoelectron momentum distribution offers a new perspective to look into molecular structures.

PACS numbers: 42.50.Hz 42.65.Re 82.30.Lp

I. INTRODUCTION

Photoionization of atoms and molecules in strong laser fields has been one of the most active projects in ultrafast physics for decades [1]. According to the Keldysh parameter [2], the ionization in strong laser fields can be understood based on the multiphoton and tunneling pictures. Photoionization carries the target information, therefore it has been successfully used to image molecules. To name a few, Meckel *et al.* extracted N_2 and O_2 molecular orbitals by subtracting photoelectron momentum distributions from differently aligned molecules [3]. Ergler *et al.* retrieved the nuclear vibration by measuring the time-delay dependent Coulomb explosion fragment [4]. Blaga *et al.* demonstrated that the very precise molecular bond length can be determined by diagnosing the photoelectron information [5].

Strong laser fields steer photoelectrons in the laser polarization plane, meanwhile imprint the field information in the photoelectron momentum distribution [6–8]. In tunneling regime, the direct ionized and rescattered electrons have broad energy spectra with the cutoff $2U_p$ and $10U_p$, respectively, where U_p is the ponderomotive energy [9]. Besides the photoelectron momentum distribution in the laser polarization plane, the lateral photoelectron momentum distribution (LPMD) has also attracted attention recently [10–13]. For atoms ionized by a circularly polarized laser pulse, the LPMD is Gaussian and its width increases with the square root of the electric field strength [14]. The LPMD will gradually transform from the smooth Gaussian to cusplike structure by varying the laser ellipticity from linear to circular polarization [13], in which the Coulomb focusing [15] is more and more important. The lateral momentum distribution of a bound electron is very important for the low-energy structure [16, 17]. For a linear molecule, whose axis is parallel to the laser polarization axis, the LPMD shows similar structures as atomic cases [3, 18]. Yurchenko *et al.* [19] studied the LPMD of H_2^+ in the case that the molecular axis is perpendicular to the laser polarization axis, and they observed the double-slit interference pattern after the rescattered electron passes through the diatomic Coulomb potential, in which the LPMD can be used to extract the internuclear distance at the rescattering timing. Most recently, Petersen *et al.* [12] calculated the LPMD of polymolecules, and demonstrated that the LPMD may have nodal planes and the lateral width of the LPMD provides useful information for molecular orbitals.

In this paper, We study the photoionization of H_2^+ in a strong linear polarized laser field, whose polarization axis is parallel to the molecular axis. In critical internuclear distances where the charge-resonance enhanced ionization (CREI) [20, 21] is very prominent, the LPMD shows distinct structures: a central disk with the largest probability density is surrounded by one or more concentric circles. The time-dependent Schrödinger equation (TDSE) simulation shows that the interatomic Coulomb potential works as a circular aperture, which diffracts the electron when it tunnels between two nuclei.

II. NUMERICAL MODELS

The photoionization of H_2^+ in strong laser fields is governed by the TDSE (atomic units are used throughout unless stated otherwise)

$$i\frac{\partial}{\partial t}\Psi(z,\rho;t) = \left[-\frac{1}{2}\frac{\partial^2}{\partial z^2} - \frac{1}{2}\left(\frac{1}{\rho}\frac{\partial}{\partial\rho} + \frac{\partial^2}{\partial\rho^2}\right) - \sum_{s=\pm1}\frac{1}{\sqrt{\rho^2+(z-sR/2)^2}} + zE(t)\right]\Psi(z,\rho;t), \quad (1)$$

*Electronic address: fhe@sjtu.edu.cn

where R is the internuclear distance. In our model, we fixed R at selective values. The linearly polarized laser field E is defined as $E = -\frac{1}{c}\frac{\partial A(t)}{\partial t}$ with c being the light velocity, where the laser vector potential is written as

$$A(t) = A_0 \cos(\omega t)\cos^2(\pi t/\tau),\ -\tau/2 < t < \tau/2. \quad (2)$$

In order to analyze the simulation results easier, we implemented an ultrashort laser pulse having $\tau = 2T$ with T being the period. The laser wavelength is 3000 nm, and the intensity is 1.5×10^{14}W/cm^2 (corresponding to $A_0 = 589$ a.u.). We used the Crank-Nicolson method to propagate the wave packet, and the initial state was obtained by imaginary time propagation [22]. We sampled the simulation box by the grids 3000×10000 in ρ-z plane and the spatial grids $\Delta\rho = \Delta z = 0.3$. The convergency has been tested by reducing the spatial grids to 0.2 a.u., which does not bring any visible difference. Under the irradiation of the laser pulse, H_2^+ has the probability to be ionized. During the interaction, the bound states stay close to the nuclei, while the freed states propagate away from nuclei. After the laser pulse is finished, we kept propagating the wave function until the bound and freed states clearly separated in space. Our simulation box is large enough to hold all wave packets, therefore no wave function hits the boundaries of the simulation box in whole calculations. To qualitatively analyze the photoelectron momentum, we removed the wavepacket in the area $r = \sqrt{\rho^2 + z^2} < 50$ a.u., and did the Fourier transformation along z-axis and the Hankel transformation along ρ-axis for the remaining wave function, i.e.,

$$\tilde{\psi}(p_\rho, p_z) = \sqrt{2\pi}\int\int \rho d\rho\ dz\varphi(\rho, z; t_f)e^{-ip_z z}J_0(p_\rho\rho), \quad (3)$$

where J_0 is the Bessel function of the first kind of zeroth order, t_f is the final time. Note that $\varphi(\rho, z; t_f)$ distributes in the area $r > 50$ a.u. and represents the ionized part. Finally, the LPMD is $\int |\tilde{\psi}(p_\rho, p_z)|^2 dp_z$. We set the boundary for bound and freed states at r=50 a.u. because they are separated very well around r=50 a.u.. Actually, we have tested that by varying the boundary between 40 and 60 a.u., the physical results do not change. We may also point that we did not chop out the states in the area $r < 50$ a.u. when an infinite laser pulse was used. In that case, the ionized electron keeps flowing out and the freed and bound states have no clear separation in space.

III. SIMULATION RESULTS

Figure 1 (a) and (b) show the LPMD when the internuclear distances are 6 and 9 a.u., respectively. We resolved the LPMD into the $\rho - \alpha$ plane where α is the polar angle. When the internuclear distance is shorter than 7 a.u., the LPMD shows a cusplike structure with a maximum at $p_\rho = 0$, which is very similar to atomic

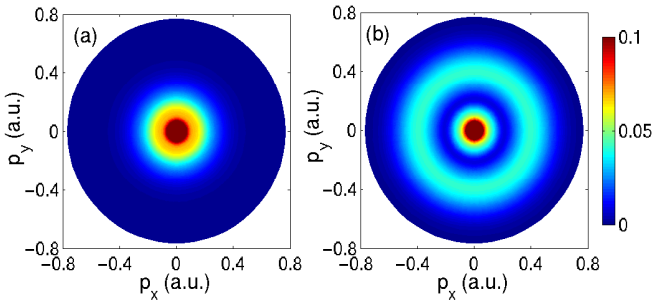

FIG. 1: (color online) The LPMD when the internuclear distance is (a) 6 a.u. and (b) 9 a.u.

cases. However, when the internuclear distance is 9 a.u., the LPMD is distinct: the central part, which is analogous to atomic cases, is surrounded by a ring with a radius around $p_\rho = 0.4$ a.u. Fig. 1 (b) looks very much like the Fraunhofer diffraction by a circular aperture: an airy disk and a secondary ring. When the internuclear distance is larger than 14 a.u., more than one ring out of the central disk are faintly seen (not shown). However, with a static electric field, several rings can be clearly seen. We will come back to this point later.

We named p_m as the momentum at the minimum between the central airy disk and the secondary ring, and plotted p_m as a function of the internuclear distance R in Fig. 2 (a), where the horizontal axis starts from $R = 8$ because no secondary ring is clearly seen when $R \leq 7$ a.u.

For diatomic molecules, the ionization probability sensitively depends on the internuclear distance. With the above given laser parameters, we reproduced the two peaks of CREI, as shown by the blue solid curve in Fig. 2 (b). The red dashed curve in Fig. 2 (b) presents the partial ionization probability where only the photoelectron with $p_\rho < p_m$ is counted. One may clearly see that the second peak is mainly contributed by the secondary ring in Fig. 1 (b). With this, one may expect that the second peak located around R=9 a.u. will be partially suppressed when the electron movement is restricted along the molecular axis [23].

The Fraunhofer-like diffraction pattern and the increasing of p_m with the increasing of R suggest a picture that the ring structure in Fig. 1 (b) is due to the diffraction when the electron propagates in the diatomic Coulomb potential. In order better to compare with the standard Fraunhofer diffraction, we adopted a static electric field instead of an alternative laser electric field for H_2^+ [24, 25]. Our test simulations showed more rings are easier to be observed for a larger internuclear distance. Therefore, we set $R = 14$ a.u. for the following demonstration. The electric amplitude is 0.053 a.u. and the field points to $+z$ axis. Fig. 3 (a) is the addition of several electron distribution snapshots at different time. Such a treatment may smear out some time-dependent fluctuation and obtain a steady electron distribution un-

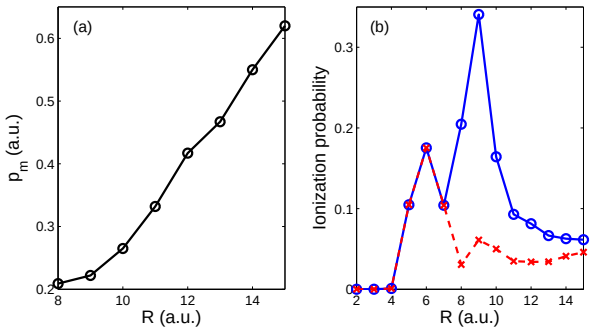

FIG. 2: (color online) (a) The momentum at the minimum between the central disk and the secondary ring as a function of the internuclear distance. (b) The total (blue solid line) and partial (red dashed line) ionization probability as a function of the internuclear distance.

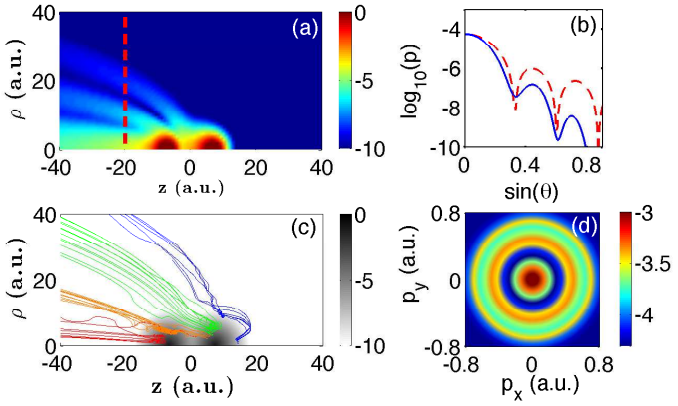

FIG. 3: (color online) (a) The electron distribution after adding several snapshots at different time. See text. (b) The spatial distribution (blue solid curve) for the emitted electron passing through $z = -20$ a.u.. θ is the scattering angle. The red dashed curve expresses the scaled Fraunhofer diffraction formula. (c) The Bohmian trajectories finally having radial momentum in different diffraction peaks. (d) The finally photoelectron momentum distribution calculated by Bohmian theories.

der the interaction of the static electric field. The wave function distribution in a transverse plane at a certain z, for example, the red vertical dashed curve in Fig. 3 (a), represents the accumulated probability passing through this plane within a certain time period. Several stripes in Fig. 3 (a) are clearly seen. We plotted the radial distribution at $z = -20$ a.u. as a function of $\sin\theta$ by the blue solid curve in Fig. 3 (b). Here, the scattering angle θ is defined as the angle for the emitted electron direction to the molecular axis. For a standard Fraunhofer diffraction by a circular aperture, the diffracted light intensity distribution is formulated $\propto (\frac{2J_1(q\sin\theta)}{q\sin\theta})^2$ where q is the product of a light wave number and the aperture radius. For comparison, we presented such an analytical formula in Fig. 3 (b) by the red dashed curve, which was scaled in order to make two curves overlap at $\theta = 0$. q was set as 11.7. The agreement of these two curves convinces us that the photoelectron spatial distribution roughly follows the rule of Fraunhofer diffraction by a circular aperture.

The followed question will be when and how the electron is diffracted to construct rings either in spatial or momentum distribution. To see that, we showed some typical Bohmian trajectories [26–29] in Fig. 3 (c). The trajectories (z, ρ) were obtained by solving the following equation

$$\frac{dz}{dt} = v_z(z, \rho; t), \quad (4)$$

$$\frac{d\rho}{dt} = v_\rho(z, \rho; t), \quad (5)$$

where the velocity fields $(v_z(z, \rho; t), v_\rho(z, \rho; t))$ are determined by the phase gradient of the wave function, i.e.,

$$v_z(z, \rho; t) = \mathrm{Im}[\frac{1}{\psi}\frac{\partial\psi}{\partial z}], \quad (6)$$

$$v_\rho(z, \rho; t) = \mathrm{Im}[\frac{1}{\psi}\frac{\partial\psi}{\partial \rho}]. \quad (7)$$

The four bunches of trajectories (from bottom to up: red, orange, green and blue curves) finally end with different radial momenta, belonging to different rings. Bohmian trajectories clearly show how the electron flows out from the nuclei. Initially, the electron equally distributes on two nuclei, shown by the gray clouds in Fig. 3 (c). When the external field is added, the Coulomb potential is distorted, as shown in Fig. 4 (b). The potential in one nuclear side is lifted up, and in the other side is lower. The two nuclei in such a distorted potential are called the up-field core and down-field core, respectively. In CREI, the electron locates in the up-field core will release from the nuclei quickly, contributing the enhanced ionization [30]. Following the Bohmian trajectories, one may figure out the flow of the electron wave packets in the laser-dressed Coulomb field. Most of red group curves in Fig. 3 (c) start from the left nuclear side when $R = 14$ a.u., which is similar to the atomic tunneling ionization. The orange group curves starting from the right nucleus are scattered by the interatomic Coulomb field and the left nucleus, ultimately joining the secondary ring. The blue and green group curves are already diffracted before they approach the left nucleus. The final momentum distribution given by the Bohmian theory is shown in Fig. 3 (d). The central disk together with several concentric rings are clearly visible.

The Bohmian trajectories in Fig. 3 (c) validate that before the electron approaches the left nucleus, the radial momenta for different trajectories have already been established. Therefore, we conclude the R-dependent LPMD is very related to the structure of the interatomic Coulomb potential. In Fig. 4 (a), we plotted the contour planes of the field-free Coulomb potential with the isosurface value being -0.35 a.u. The three contour planes

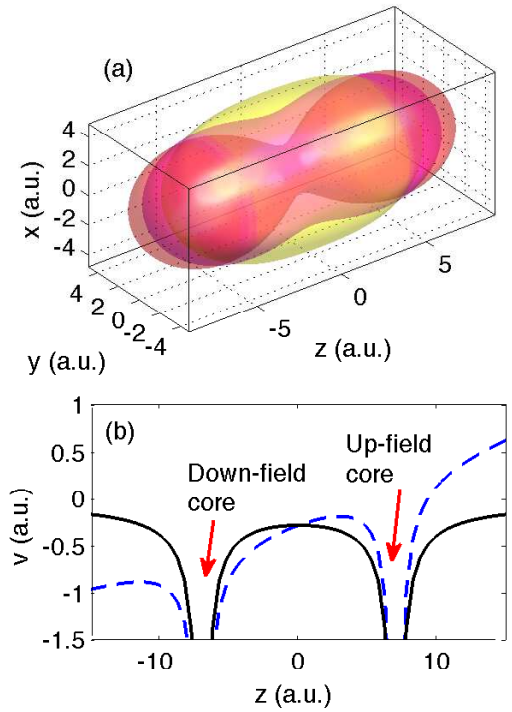

FIG. 4: (color online) (a) Contour planes (the isosurface value is -0.35 a.u.) for the internuclear distance R=6 (yellow), 9 (red), 11 (magenta) a.u.. (b) The field-free (black solid curve) and field-dressed(blue dashed curve) Coulomb potential in the plane $\rho = 0$. The instantaneous field amplitude is 0.053 a.u. and points to the $+z$ direction.

are for the internuclear distances R=6, 9, 11 a.u., respectively. Fig. 4 (b) shows the field-free (black solid curve) and field-dressed (red dashed curve) Coulomb potential in the plane $\rho = 0$ for R=9 a.u. The contour plane in the middle of two nuclei works as a tube, inside which the potential is lower therefore the electron may tunnel through. The radius of the tube is larger for a smaller internuclear distance. When the internuclear distance is less than 6 a.u., the tube is wide and the electron is less restricted, thus almost no diffraction happens and the LPMD has a similar shape with atomic cases. For a larger internuclear distance, the contour plane in the middle of the two nuclei shrinks more. Thus, when the electron tunnels through such a shrunk tube, it is analogous to pass a small aperture and diffraction becomes very important. A larger internuclear distance deduces a smaller tube connecting two nuclei, which leads to a larger diffraction angle. This phenomenological explanation is consistent with the simulation results shown in Fig. 2 (a). The static field is easier than the alternative laser electric field to produce multiple rings when the internuclear distance is very long. This is because the interatomic barrier is already very high or the tube is broken, and tunneling between two nuclei driven by the alternative laser electric field is extremely hard. With this, we explain why the Fraunhofer-like diffraction pattern in the LPMD is most prominent for the internuclear distance where the second peak of CREI locates.

IV. DISCUSSIONS AND CONCLUSIONS

In our simulations, the internuclear distance is only a parameter, and has no dynamical contribution. One question would be whether this Fraunhofer-like diffraction pattern will survive in a moving-nuclei system. We expect the LPMD explored in this paper should still be measurable for a dissociating H_2^+. With the cold target recoil ion momentum spectroscopy [31, 32], the electron and nuclei can be coincidentally recorded. From the kinetic energy release of the nuclei, one may retrieve the internuclear distance. Therefore, the LPMD associated with a particularly internuclear distance can be identified, and the average for internuclear distances is not necessary any more. Compared to the electron, we do not expect the ultraslow movement of the nuclei will alter the LPMD.

We also ran simulations using a 2000 nm laser pulse, and we obtained similar LPMD. For laser pulses with even shorter wavelengths but similar intensities, the tunneling character is less and less prominent, and we found the central disk and the secondary ring in the LPMD slowly merge together. Since the midinfrared laser pulses have already been well established [33], we expect this LPMD can be observed very soon in experiment. By the way, the double peaks in CREI are more obvious by implementing a laser pulse with a longer wavelength.

The LPMD has the potential to image molecular structures. The radius of the rings in the LPMD carries the information of internuclear distances, i.e., a larger diffraction angle in the LPMD indicates a smaller aperture, thus a longer internuclear distance. For a larger molecule with more than two Coulombic centers, such as C_2H_2, the diffraction might be more complex when the electron tunnels along the molecular axis. But the test simulations show the Fraunhofer-like diffraction pattern is still preserved. The LPMD has the advantage to image molecular structure because the LPMD is less distorted by the laser field, but mainly determined by the target structure.

In conclusion, when the internuclear distance of H_2^+ is critical that the CREI is most prominent, the LPMD presents a central disk surrounded by one or several rings. The enhanced ionization probability is mainly donated by the electron in the rings. By comparing the LPMD with a standard Fraunhofer diffraction by a circular aperture, we explore the diffraction process: the electron is diffracted when it moves from the up-field core toward the down-field core by penetrating the stretched molecular interatomic Coulomb potential, which works as a circular aperture. Since the CREI is general in molecules, we believe the Fraunhofer-like

diffracted LPMD can be observed in many molecules. The LPMD offers a new perspective to reconstruct the internuclear distance, molecular Coulomb potential, as well as other molecular information.

acknowledgements

This work was supported by NSF of China (Grant No. 11104180, 11175120, 11121504, 11322438), and the Fok Ying-Tong Education Foundation for Young Teachers in the Higher Education Institutions of China (Grant No. 131010).

[1] F. Krausz and M. Ivanov, Attosecond physics, Reviews of Modern Physics **81**, 163–234 (2009).

[2] L. V. Keldysh, Ionization in the Field of a Strong Electromagnetic Wave, Sov. Phys. JETP **20**, 1307 (1965).

[3] M. Meckel, D. Comtois, D. Zeidler, A. Staudte, D. Pavičić, H. C. Bandulet, H. Pépin, J. C. Kieffer, R. Dörner, D. M. Villeneuve, and P. B. Corkum, Laser-Induced Electron Tunneling and Diffraction, Science **320**, 1478 (2008).

[4] Th. Ergler, B. Feuerstein, A. Rudenko, K. Zrost, C. D. Schröter, R. Moshammer, and J. Ullrich, Quantum-phase resolved mapping of ground-state vibrational d_2 wave packets via selective depletion in intense laser pulses, Phys. Rev. Lett. **97**, 103004 (2006).

[5] C. I. Blaga, J. Xu, A. D. DiChiara, E. Sistrunk, K. Zhang, P. Agostini, T. A. Miller, L. F. DiMauro, and C. D. Lin, Imaging ultrafast molecular dynamics with laser-induced electron diffraction, Nature **483**, 194 (2012).

[6] Y. Mairesse, F. Quéré, Frequency-resolved optical gating for complete reconstruction of attosecond bursts, Phys. Rev. A **71**, 011401(R) (2005).

[7] F. Lindner, M. G. Schätzel, H. Walther, A. Baltuska, E. Goulielmakis, F. Krausz, D. B. Milosevic, D. Bauer, W. Becker, G. G. Paulus, Attosecond double-slit experiment, Phys. Rev. Lett. **95**, 040401 (2005).

[8] T. Wittmann, B. Horvath, W. Helml, M. G. Schätzel, X. Gu, A. L. Cavalieri, G. G. Paulus and R. Kienberger, Single-shot carrier-envelope phase measurement of few-cycle laser pulses, Nature Physics **5**, 357 (2009).

[9] C. D. Lin, A. T. Le, Z. Chen, T. Morishita and R. Lucchese, Strong field rescattering physics – self-imaging of a molecule by its own electrons, J. Phys. B **43**, 122001 (2010)

[10] A. Rudenko, K. Zrost, Th. Ergler, A. B. Voitkiv, B. Najjari, V. L. B. de Jesus, B. Feuerstein, C. D. Schröter, R. Moshammer, and J. Ullrich, Coulomb singularity in the transverse momentum distribution for strong-field single ionization, J. Phys. B **38**, L191 (2005).

[11] J. Henkel, M. Lein, V. Engel, and I. Dreissigacker, Adiabaticity in the lateral electron-momentum distribution after strong-field ionization, Phys. Rev. A **85**, 021402 (2012).

[12] I. Petersen, J. Henkel, and M. Lein, Signatures of molecular orbital structure in lateral electron momentum distributions from strong-field ionization, Phys. Rev. Lett. **114**, 103004 (2015).

[13] I. A. Ivanov, Evolution of the transverse photoelectron-momentum distribution for atomic ionization driven by a laser pulse with varying ellipticity, Phys. Rev. A **90**, 013418 (2014).

[14] L. Arissian, C. Smeenk, F. Turner, C. Trallero, A. V. Sokolov, D. M. Villeneuve, A. Staudte, and P. B. Corkum, Direct test of laser tunneling with electron momentum imaging, Phys. Rev. Lett. **105**, 133002 (2010).

[15] T. Brabec, M. Yu. Ivanov, and P. B. Corkum, Coulomb focusing in intense field atomic processes, Phys. Rev. A **54**, R2551–R2554 (1996).

[16] W. Quan, Z. Lin, M. Wu, H. Kang, H. Liu, X. Liu, J. Chen, J. Liu, X. T. He, S. G. Chen, H. Xiong, L. Guo, H. Xu, Y. Fu, Y. Cheng, and Z. Z. Xu, Classical Aspects in Above-Threshold Ionization with a Midinfrared Strong Laser Field, Phys. Rev. Lett. **103**, 093001 (2009).

[17] C. I. Blaga, F. Catoire, P. Colosimo, G. G. Paulus, H. G. Muller, P. Agostini and L. F. DiMauro, Strong-field photoionization revisited, Nature Physics **5**, 335 (2008).

[18] Q. Ji, S. Cui, X. You, X. Gong, Q. Song, K. Lin, H. Pan, J. Ding, H. Zeng, F. He, and J. Wu, Orbital-resolved strong-field single ionization of acetylene, Phys. Rev. A , in press.

[19] S. N. Yurchenko, S. Patchkovskii, I. V. Litvinyuk, P. B. Corkum, and G. L. Yudin, Laser-induced interference, focusing, and diffraction of rescattering molecular photoelectrons, Phys. Rev. Lett. **93**, 223003 (2004).

[20] T. Seideman, M. Yu. Ivanov, and P. B. Corkum, Role of Electron Localization in Intense-Field Molecular Ionization, Phys. Rev. Lett. **75**, 2819 (1995).

[21] T. Zuo and A. D. Bandrauk, Charge-resonance-enhanced ionization of diatomic molecular ions by intense lasers, Phys. Rev. A **52**, R2511–R2514 (1995).

[22] R. Kosloff and H. Tal-Ezer, A direct relaxation method for calculating eigenfunctions and eigenvalues of the schrödinger equation on a grid, Chemical Physics Letters, **127**, 223 (1986).

[23] H. Xu, F. He, D. Kielpinski, R. T. Sang and I. V. Litvinyuk, Experimental observation of the elusive double-peak structure in R-dependent strong-field ionization rate of H_2^+, Sci. Rep. **5**, 13527 (2015).

[24] M. Plummer and J. F McCann, Field-ionization rates of the hydrogen molecular ion, J. Phys. B **29**, 4625, (1996).

[25] Ts. Tsogbayar and M. Horbatsch, Calculation of stark resonance parameters for the hydrogen molecular ion in a static electric field, J. Phys. B **46**, 085004 (2013).

[26] N. Takemoto and A. Becker, Visualization and interpretation of attosecond electron dynamics in laser-driven

hydrogen molecular ion using bohmian trajectories, The Journal of Chemical Physics **134**, 074309 (2011).

[27] Y. Song, F. Guo, S. Li, J. Chen, S. Zeng, and Y. Yang, Investigation of the generation of high-order harmonics through Bohmian trajectories, Phys. Rev. A **86**, 033424 (2012).

[28] R. Sawada, T. Sato, and K. L. Ishikawa, Analysis of strong-field enhanced ionization of molecules using Bohmian trajectories, Phys. Rev. A **90**, 023404 (2014).

[29] H. Z. Jooya, D. A. Telnov, P. Li, and S. Chu, Exploration of the subcycle multiphoton ionization dynamics and transient electron density structures with Bohmian trajectories, Phys. Rev. A **91**, 063412 (2015).

[30] J. Wu, M. Meckel, L. Ph. H. Schmidt, M. Kunitski, S. Voss, H. Sann, H. Kim, T. Jahnke, A. Czasch and R. Dörner, Probing the tunnelling site of electrons in strong field enhanced ionization of molecules, Nat. Commun. **3**, 1113 (2012)

[31] R. Dörner, V. Mergel, O. Jagutzki, L. Spielberger, J. Ullrich, R. Moshammer, and H. Schmidt-Böcking, Cold Target Recoil Ion Momentum Spectroscopy: a 'momentum microscope' to view atomic collision dynamics, Phys. Rep. **330**, 95 (2000).

[32] J. Ulrich, R. Moshammer, A. Dorn, R. Dörner, L. Ph. H. Schmidt, and H. Schmidt-Böcking, Recoil-ion and electron momentum spectroscopy: reaction-microscopes, Rep. Prog. Phys. **66**, 1463 (2003).

[33] A. D. DiChiara, S. Ghmire, D. A. Reis, L. F. DiMauro, P. Agostini, in *Attosecond Physics*, editored by L. Plaja, R. Torres, A. Zaïr (Springer Berlin Heidelberg, 2013) , pp. 81-98